Journal of Power Sources 329 (2016) 262–267

Contents lists available at ScienceDirect

Journal of Power Sources

journal homepage: www.elsevier.com/locate/jpowsour

A high temperature study on thermodynamic, thermal expansion and electrical properties of $BaCe_{0.4}Zr_{0.4}Y_{0.2}O_{3-\delta}$ proton conductor

J.F. Basbus [a, *], M.D. Arce [a], F.D. Prado [b], A. Caneiro [a], L.V. Mogni [a]

[a] CNEA-CONICET, Centro Atómico Bariloche, Av. Bustillo 9500, S. C. de Bariloche, Rio Negro, 8400, Argentina
[b] Departamento de Física, Universidad Nacional de Sur, and Instituto de Física, CONICET, Alem 1253, Bahía Blanca, 8000, Argentina

HIGHLIGHTS

- BCZY was synthesized by solid state reaction and sintered at 1600 °C 12 h.
- Proton incorporation was studied under O_2 and H_2 atmospheres between RT and 950 °C.
- The bulk conductivity of BCZY was independent regardless wet atmosphere.
- Grain boundary conductivity strongly depends on atmosphere nature and thermal history.
- Conductivity change between H_2O and D_2O O_2 atmosphere reveals protonic conductivity.

ARTICLE INFO

Article history:
Received 21 March 2016
Received in revised form
28 July 2016
Accepted 18 August 2016
Available online 27 August 2016

Keywords:
PC-SOFC
$BaCe_{0.4}Zr_{0.4}Y_{0.2}O_{3-\delta}$ electrolyte
Proton incorporation
Bulk conductivity
Grain boundary conductivity
Isotopic effect

ABSTRACT

$BaCe_{0.4}Zr_{0.4}Y_{0.2}O_{3-\delta}$ (BCZY) was synthesized by solid state reaction, calcined and sintered at 1600 °C for 12 h. Crystal structure was studied by X-ray diffraction (XRD). Morphology and porosity were determined by scanning electron microscopy (SEM). Crystalline structure, oxygen non-stoichiometry, linear expansion and electrical conductivity were characterized under oxidizing and reducing atmosphere by high temperature X-ray diffraction (HT-XRD), thermogravimetry (TG), dilatometry, and electrochemical impedance spectroscopy (EIS), respectively. Chemical stability under CO_2-rich atmosphere was evaluated by TG. BCZY electrical conductivity was studied by EIS under O_2-containing atmosphere with water vapor (2% H_2O) and heavy water vapor (2% D_2O) in order to evaluate protonic conductivity. Throughout these techniques, interstitial proton incorporation/loss was observed under oxidizing and reducing atmosphere, between 300 and 500 °C. The conductivity presents two contributions. The bulk conductivity at high frequencies takes the same value regardless wet oxidizing or reducing atmosphere, decreasing its value in presence of D_2O vapor supporting H-conductivity. On the other hand, the grain boundary conductivity was strongly dependent on the nature of wet atmosphere.

1. Introduction

Barium cerates and zirconates oxides are capable of transporting protons through their crystal lattice [1,2]. This feature makes them potential candidates as hydrogen sensors, membranes for hydrogen purification and isotopic exchange (hydrogen, deuterium, tritium -H/D/T-) [3], and electrolyte for proton conductor solid oxide fuel cell (PC-SOFC) and solid oxide electrolyzer cell (PC-SOEC) [4].

Recently, $BaCe_{0.4}Zr_{0.4}Y_{0.2}O_{3-\delta}$ compound (BCZY) was proposed as material for these applications [5–9]. BCZY presents high intra-granular (bulk) protonic conductivity and excellent CO_2 tolerance. However, proton conducting perovskites exhibit in certain cases high sintering temperature (1500–1700 °C) and low inter-granular (grain boundary) protonic conductivity. High CO_2 tolerance and suitable transport properties make BCZY a good electrolyte for anode supported PC-SOFC [10] when using low purity H_2 as fuel. Regardless the potential applications of this compound, non-detailed characterization was performed to date with the aim to obtain fundamental understanding about the behavior of this material under different operating conditions. In this work, high temperature properties of BCZY, such as crystalline structure, non-stoichiometry, linear expansion and electrical resistance are presented under both H_2- and O_2- rich atmospheres.

* Corresponding author.
E-mail address: basbus@cab.cnea.gov.ar (J.F. Basbus).

http://dx.doi.org/10.1016/j.jpowsour.2016.08.083
0378-7753/

2. Experimental

$BaCe_{0.4}Zr_{0.4}Y_{0.2}O_{3-\delta}$ (BCZY) perovskite was synthesized by solid state reaction (SSR) from stoichiometric amounts of $BaCO_3$, CeO_2, ZrO_2 and Y_2O_3. The precursors were ball milled, calcined at 1350 °C for 4 h and sintered at 1600 °C 12 h. In cases where powders were required, sinteredpellets were grinded in mortar. Phase purity was evaluated by X-ray diffraction (XRD), by using PANalytical Empyrean diffractometer with Cu Kα radiation, a graphite monochromator and a PIXcel^{3D} detector.

Structural and microstructural parameters were obtained from the diffraction pattern of BCZY powders by using the Rietveld method and the FullProf Suite software [11]. The instrumental line broadening was obtained from a pattern of Y_2O_3. All reflection peaks of BCZY were indexed according to the cubic symmetry, space group *Pm-3m*, N° 221 [5,6,12], previously reported. The microstructural parameters, such as crystallite size and microstrain effect, were calculated by using the Scherrer formula and isotropic microstructural model, respectively.

Microstructure of BCZY sintered pellets was observed by scanning electron microscopy (SEM) with a Philips 515 microscope. Elemental analysis was carried out by using energy dispersive spectroscopy (EDS). The porosity was analyzed from SEM images of polished cross sections of a sample by using ImageTool3 software [13–15]. In order to determine open and close porosity, the sample density was measured by hydrostatic weighing using a Cahn 1000 electrobalance [16] and diethyl phthalate as the immersion fluid, as described elsewhere [17].

Crystal structure as a function of temperature was studied by XRD, between room temperature and 900 °C under a mixture of ~80% N_2 and ~20% O_2 (synthetic air). Diffraction patterns of BCZY powders at high temperatures were collected by using an Anton Paar camera coupled to the PANalytical Empyrean diffractometer. Structural and experimental parameters at high temperatures were obtained by the Rietveld method, using sequential mode of the FullProf Suite software [11].

Thermodynamic stability of BCZY powder was studied by thermogravimetry (TG), making use of a Cahn 1000 electrobalance [16]. Mass variation (% Weight) was analyzed by thermal cycling the powder from room temperature to 1000 °C at heating/cooling rate of 1 °C min^{-1} under 20% O_2/Ar, followed by a second cycle under 10% H_2/Ar atmospheres. Also, CO_2 tolerance was evaluated by an ageing test under 10% CO_2/Ar, between room temperature and 1000 °C, at a heating/cooling rate of 5 °C min^{-1}.

Linear expansion coefficient of BCZY sintered pellet was determined by dilatometry, between room temperature and 900 °C, under atmospheric air and 5% H_2/Ar at a heating/cooling rate of 1 °C min^{-1}. The measurements were performed by using LINSEIS L75VS1000C vertical dilatometer.

Electrical conductivity of BCZY sintered pellets was determined by electrochemical impedance spectroscopy (EIS). The pellets were painted on both sides with Pt ink. Impedance spectra were collected between 100 and 600 °C, under 20% O_2/Ar and 10% H_2/Ar wet (2% H_2O vapor) atmospheres and under 20% O_2/Ar + 2% D_2O vapor. Measurements were performed by using an Autolab PGSTAT30 potentiostat/galvanostat, from 1 MHz to 0.1 Hz with 50 mV amplitude. EIS spectra were fitted with equivalent circuits (EEC), by using Zview2 software [18].

3. Results and discussion

Fig. 1 shows the diffraction pattern of BCZY powder under atmospheric air at room temperature, The X-ray data were indexed in the cubic symmetry and the *Pm-3m* space group. The lattice parameter (a), average crystallite size (d_c) and isotropic strains (IS)

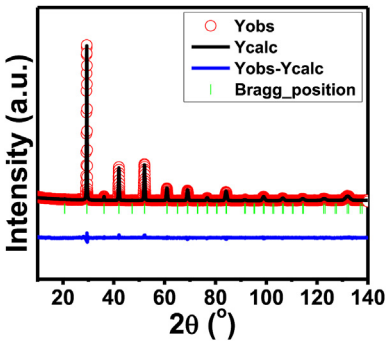

Fig. 1. X-ray diffraction pattern: experimental (○) calculated (−), difference between both (—) and Bragg positions (|) of BCZY powder under air at room temperature.

were a = 4.3022(1) Å, d_c = 357(1) nm and IS = 38.36(1) %%, respectively. This information was obtained from Rietveld refinement with a goodness of fits of R_p = 14.2, R_{wp} = 14.1 and χ^2 = 2.26. Nasani et al. [5] and Tu et al. [19] reported for this compound lattice parameters of 4.320 and 4.322 Å, respectively. These disagreements on lattice parameters could be due to different synthesis methods and/or degree of hydration (depending on storage conditions) for each sample. The incorporation of H_2O molecules into the BCZY structure can also explain the strain effects on the peak broadening due to lattice distortion.

Fig. 2a shows a SEM micrograph of a polished cross section of a

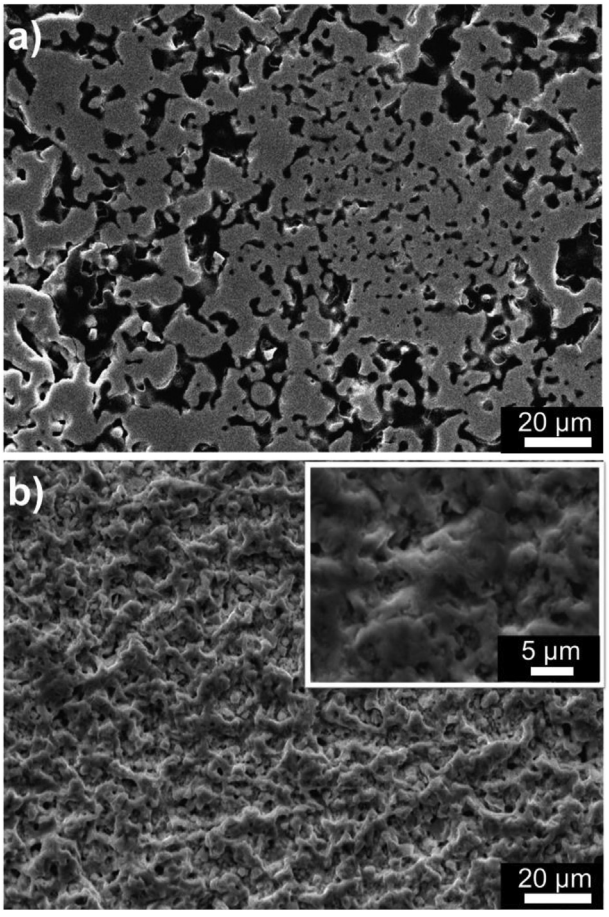

Fig. 2. SEM image of a BCZY sintered pellet, a) polished cross-section and b) front section.

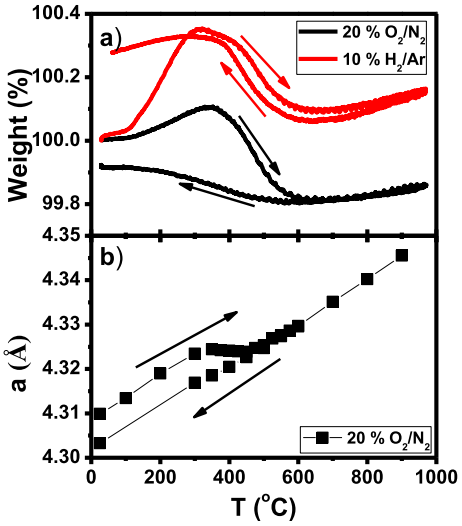

Fig. 3. a) Weight (%) and b) lattice parameters for BCZY powder as a funcion of temperature. The high temperature diffraction patterns were collected under oxidizing atmosphere, while mass changes were measured under oxidizing and reducing atmospheres.

BCZY sintered pellet. An estimated total porosity of 22(5) % and a grain size of ~ 1 μm (Fig. 2b) were determined by image analysis from the average of 5 cross section images. A density of 6.00 g/cm^3 was measured by hydrostatic weighing, which corresponds to 97% of the theoretical density (6.17 g/cm^3 based on XRD data), indicating that 3% of the pores are closed, while open porosity is of approximately 19(5)%. From Fig. 2b, liquid phase formation is not discarded but is insufficient to promote densification. The low density and small grain size achieved by SSR method do not compromise the aim of our study, which is to understand the transport properties of bulk and grain boundary, thermal expansion, oxygen non-stoichiometry under different atmospheres and the CO_2 tolerance of the BCZY compound. We discarded the use of additives in order to obtain more dense materials by the SSR method since additives could be dissolved in bulk and grain boundaries modifying the properties to be studied [20].

The protonic conductivity of an electrolyte depends on the oxygen non-stoichiometry, hydration degree of oxygen vacancies, and temperature [21]. Therefore, the hydration/dehydration process in BCZY was studied as a function of temperature under different atmospheres. Fig. 3a compares mass change of BCZY powder, under oxidizing and reducing atmosphere, between room temperature

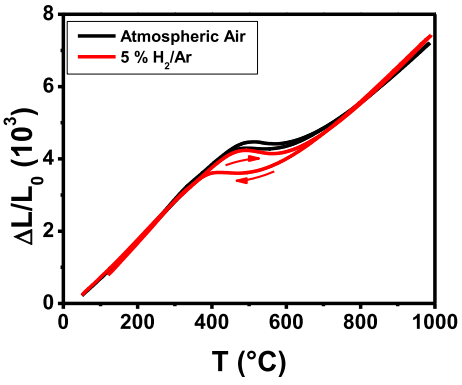

Fig. 4. Linear expansion of BCZY sintered pellet as a function of temperature under atmospheric air and 5% H_2/Ar.

Table 1
TECs of BCZY obtained by HT-XRD and dilatometry under different atmospheres.

Atmosphere	TEC (10^{-6} K^{-1})			
	HT-XRD		Dilatometry	
	20–300 °C	20–600 °C	20–350 °C	20–600 °C
Air	11.6(1)	8.0(1)	11.2(1)	7.5(1)
Dilute Hydrogen	–	–	10.4(1)	6.9(1)

and 1000 °C. TG plots indicates:

- the presence of hysteresis under both atmospheres below 600° C.
- mass gain under both atmospheres at T > 150 °C, reaching a maximum value at 350 °C and then decreases. Mass gain was higher under hydrogen than oxygen containing atmosphere.
- final mass was lower than initial one under synthetic air, while the opposite behavior was observed under diluted hydrogen

Kruth and Irvine [21] suggested for $BaCe_{1-x}Y_xO_{3-\delta}$ (x = 0.05, 0.10, 0.15) that the slope changes in TG plots were due to Ce^{+4} reduction under wet diluted hydrogen. Lyagaeva et al. [22] reported for $BaCe_{0.8-x}Zr_xY_{0.2}O_{3-\delta}$ a hysteresis under air, with a small mass loss, which is associated to kinetic causes. Our heating/cooling rate (1 °C min^{-1}) was five times lower than that used in these studies which should reduce the kinetic effect. However, the hysteresis behavior is similar. Regarding the Ce reduction, a previous work shows that $BaCeO_{3-\delta}$ is not reduced under 5% H_2 atmosphere below 800 °C, under equilibrium conditions [13]. The mass gain/loss due to the interstitial protons incorporation in the perovskite structure cause lattice distortions with the consequent modification of the

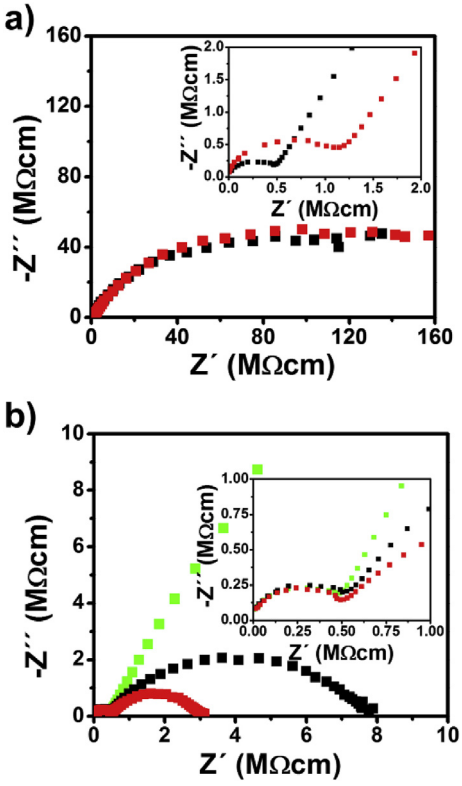

Fig. 5. Nyquist plots of BCZY sintered pellet measured at 100 °C under a) 20% O_2/Ar with H_2O vapor (■) and D_2O vapor (■), b) wet 10% H_2/Ar on heating (■) and cooling (■) run (wet 20% O_2/Ar was included (■) for comparison).

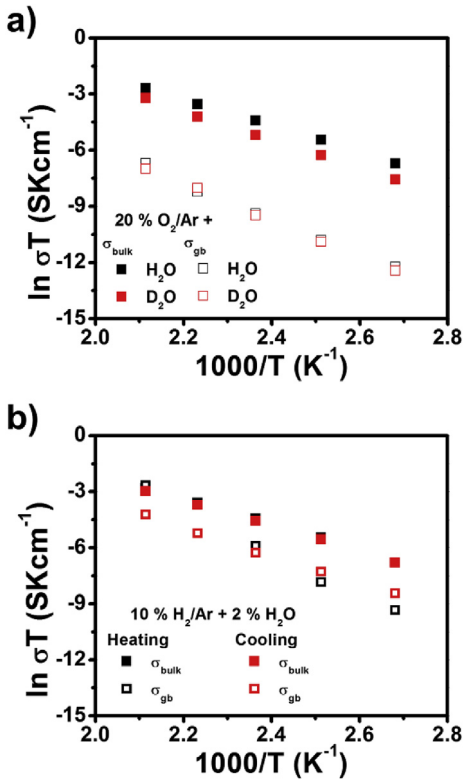

Fig. 6. Arrhenius plots for BCZY sintered pellet a) 20% O_2/Ar with H_2O vapor and D_2O, b) wet 10% O_2/Ar on heating and cooling run.

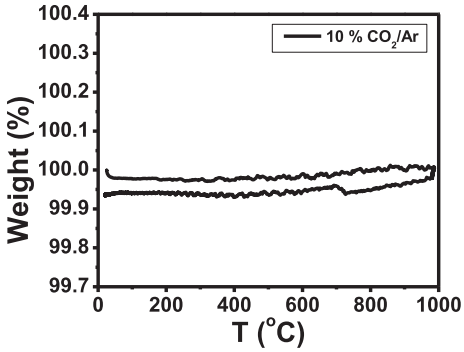

Fig. 7. Weight (%) as funcion of temperature under 10% CO_2/Ar for BCZY powder.

lattice parameters and the oxygen chemical activity. This effect was confirmed by high temperature XRD (HT-XRD). Fig. 3b shows the lattice parameters evolution of BCZY powder under synthetic air, between room temperature and 900 °C. From this Figure it was observed:

- on heating run: a positive slope (cell expansion) between room temperature and ~300 °C, a slightly negative slope (cell shrinkage) between 300 and 500 °C, and a positive slope, similar to the first one, between 500 and 900 °C.
- on cooling run: a unique positive slope, with the same value than that of the heating run between 500 and 900 °C.

The slightly negative slope on heating run between 300 and 500 °C could be due to dehydration of oxygen vacancies. No slope changes between these temperatures on cooling run confirms this assumption, i.e. all H_2O was removed from the structure. Also, the lattice parameters after cycling were lower than the initial ones, indicating hydration during sample storage. Furthermore, H_2O gain/loss modifies the oxygen activity, and introduces lattice distortions.

Fig. 4 displays the linear expansion ($\Delta L/L_0$) of BCZY sintered pellet between room temperature and 950 °C, under atmospheric air and 5% H_2/Ar (ΔL is the length change and L_0 the initial length at 20 °C). Under both atmospheres a hysteresis was identified, between ~400 and 600 °C, although the hysteresis was more prominent under reducing atmosphere with slightly wider temperature range. These results show the same trend seen on TG and HT-XRD measurements. Gorbova et al. and Yamaguchi et al. observed this behavior for $BaCe_{1-x}Sm_xO_{3-\delta}$ and $BaCe_{1-x}Yb_xO_{3-\delta}$ systems ($x = 0-0.2$), respectively [23,24]. They assumed that a phase transitions is the responsible of non-linear dependences, which is more evident as Sm and Yb content increases. Zhou et al. also suggested for $BaZr_{0.1}Ce_{0.7}Y_{0.1}Yb_{0.1}O_{3-\delta}$ compound structural transformations or phase changes between 500 and 800 °C, under air and Ar [25]. However, the high temperature diffraction patterns of BCZY collected in this work did not evidenced phase transitions, but only changes on lattice parameters associated to sample dehydration. Lagaeva et al. observed for $BaCe_{0.4}Zr_{0.2}Y_{0.2}O_{3-\delta}$, that linear expansion depends on pH_2O and not on pO_2 [12]. The behavior observed by Lagaeva et al. is in agreement with our assumption that proton incorporation/loss in the structure is the responsible of the observed hysteresis for TG, HT-XRD and linear expansion measurements. Table 1 summarizes the TEC values under both atmospheres, which were similar to those reported by Lyagaeva et al. [22] and other compositions [26]. The similar TEC values for BCZY under both atmospheres improve the mechanical stability of BCZY electrolyte membranes separating reduced and oxidizing atmospheres. These TEC values perfectly match with those of anode materials (10.10^{-6} K^{-1} [27]), but they are lower than those of most commonly used SOFC cathodes ($>20.10^{-6}$ K^{-1} [4]).

Transport mechanism of protonic conductors is given by hopping of interstitial protons between oxygen sites [2,28,29]. A good protonic conductor electrolyte should present negligible electron transport number (t_e) compared to ion transport number (t_i), in order to minimize leakage current. Therefore, total electrical conductivity should be a representative measurement of the ionic conductivity. Fig. 5a compares Nyquist plots of BCZY sintered pellet under water vapor (2% H_2O) and heavy water vapor (2% D_2O) 20% O_2/Ar at 100 °C. Similar results were obtained between 100 and

Table 2
Resistances, capacitances, maximum frequencies and activation energies under different atmospheres at 100 °C.

Atmosphere		Bulk (b)				Grain boundary (gb)			
		σ (μS cm^{-1})	C (pF cm^{-1})	f_{max} (kHz)	E_a (eV)	σ (nS cm^{-1})	C (nF cm^{-1})	f_{max} (Hz)	E_a (eV)
20% O_2/Ar	+H_2O	3.3(1)	7.0(2)	155.8	0.61(1)	13(1)	1.6(1)	2.8	0.83(3)
	+D_2O	1.4(1)	5.8(1)	83.6	0.66(1)	11(2)	1.5(3)	2.5	0.84(2)
10% H_2/Ar	+H_2O heating	3.0(1)	8.8(2)	89.9	0.60(2)	239(1)	2.6(2)	16.3	1.07(7)
	+H_2O cooling	3.0(1)	10.8(2)	57.0	0.58(1)	583(1)	4.1(3)	24.0	0.64(2)

Table 3
Comparison of distinctive properties between some selected doped Cerates and Zirconates of barium compounds.

Composition	σ (mS cm^{-1}) at 300 °C				Carbonation resistance	Porosity (%)	Sintering T (°C)	Ref.
	b	gb	Total	Conditions				
$BaCe_{0.4}Zr_{0.4}Y_{0.2}O_{3-\delta}$	2	0.1	~0.1	Wet 20% O_2/Ar	Stable under 10% CO_2	22(5)	1600	In this work
$BaCe_{0.8}Y_{0.2}O_{3-\delta}$	45	0.59	0.58	Wet N[2]	Stable until 400 °C under 100% CO_2[a]	~4	1400	[6]
$BaZr_{0.8}Y_{0.2}O_{3-\delta}$	0.54	0.13	0.1		Stable under 100% CO_2[a]	~22	1400	
$Ba(Ce_{0.75}Zr_{0.25})_{0.9}Nd_{0.1}O_{2.95}$	0.041	8.10^{-4}[b]	$\sim 8.10^{-4}$	Wet air	Stable under 100% CO_2	17	1550	[36]
$BaCe_{0.8}Zr_{0.1}Nd_{0.1}O_{3-\delta}$	0.11	1.10^{-4}[b]	$\sim 1.10^{-4}$	Wet Ar	Stable at least for short periods under 100% CO_2	>5	1650	[37]
$BaCe_{0.4}Zr_{0.4}Sc_{0.2}O_{3-\delta}$	0.16	–	–	Wet 5% H_2/Ar	Stable until 900 °C, 100% CO_2	25–30	1600	[38]
$BaZr_{0.1}Ce_{0.7}Y_{0.2}O_{3-\delta}$	–	–	~1	Wet 4% H_2/Ar	Stable at 500 °C, 2% CO_2	Fully dense	1550	[39]

[a] Fast heating rate (10 °C/min) could affect the kinetics.
[b] gb conductivity was calculated using Brick layer model.

200 °C. Both impedance spectra showed three contributions (see Fig. 6a):

- high frequency associated with ionic transport into bulk (b)
- medium frequency related to transport through the grain boundaries (gb)
- low frequency due to electrode reaction

Similarly, Fig. 5b shows Nyquist plots of BCZY under wet (2% H_2O vapor) 10% H_2/Ar, on heating and cooling run. Impedance spectra under wet 20% O_2/Ar was also included for comparison. As it was mentioned above, BCZY presented three arc circles under wet synthetic air, while on wet diluted hydrogen only two arcs were observed. These differences were due to lower polarization resistance to electrode reaction of H_2 ($H_2 \rightarrow 2H^+ + 2e^-$) than O_2 ($O_2 + 4e^- \rightarrow 2O^{-2}$). Moreover, the high frequency arcs (bulk) are independent on the atmosphere, whereas the medium frequency contribution (grain boundary) decreases between the cooling and heating runs under reducing atmosphere. This difference suggests partial reduction of Ce^{+4} into Ce^{+3} at grain boundaries at 600 °C. This reduction is not evidenced by TG measurements.

Impedance spectra were fitted with equivalent electrical circuits (EEC), where each arc was considered as an electrical resistance in parallel with a constant phase element (R//CPE). Additionally, the porosity effect was corrected on the BCZY conductivity by using the asymmetric Bruggeman model [30,31]. Table 2 summarizes relevant values obtained from the fits (resistance, capacitance, maximum frequency and activation energy) under different atmospheres at 100 °C. From Fig. 6a and b we conclude that:

- bulk conductivity was independent on the wet atmosphere nature (H_2 or O_2 containing).
- bulk conductivity was dependent on the water vapor nature (i.e., H_2O or D_2O) under oxidizing atmosphere. Bulk conductivity under water vapor was two times higher than under heavy water vapor. The higher mobility of H^+ than D^+ [32] confirms proton conductivity of BCZY under oxidizing atmosphere.
- grain boundary conductivity depends on wet atmosphere (i.e. oxidizing or reducing atmosphere) and the previous history of the material (heating/cooling run). Ce^{+4} partial reduction at grain boundaries could affect the protonic transport.

Lagaeva et al. observed for $BaCe_{1-x}Zr_xY_{0.2}O_{3-\delta}$ (x = 0–0.8) compounds that conductivity decreases with Zr content and high pO_2 introduces p-type conductivity at 600–900 °C [12]. BCZY would present mixed ionic-electron hole conductivity under oxidizing conditions and purely ionic under reducing atmospheres. Fig. 6a and b compares Arrhenius plots under different atmospheres. Activation energy values of bulk were independent on wet (H_2O) atmosphere (E_a ~0.6 eV). However, these values were slightly lower than those obtained under D_2O ($E_a = 0.66$ eV) [32]. Activation energy values for bulk were similar to those reported by Nasani et al. [5]. Moreover, activation energies for grain boundaries were different according to measurement conditions, which suggested a strong effect of the surface condition, i.e. oxidation/reduction degree of Ce.

CO_2 tolerance of an electrolyte must be guaranteed when SOFC operates under low purity fuels since surface carbonation can greatly affect the cell performance. Ageing tests were carried out under high temperature and CO_2 concentrations in order to estimate the material stability under SOFC operating condition [6,32]. Fig. 7 indicates mass variation for BCZY powder between room temperature and 950 °C under 10% CO_2/Ar, where no significant mass change was observed. This result was confirmed by XRD after CO_2 cycling, where no secondary phases were detected. Otherwise, Tu et al. [19] observed $BaCe_{0.4}Zr_{0.4}Y_{0.2}O_{3-\delta}$ decomposition under 100% CO_2 atmosphere, by in situ XRD and Raman spectroscopy. These results reveal that BCZY would be degraded under pure methane or CO_2-rich atmospheres, but it could be stable under low quality hydrogen fuel, i.e. between 10 and 20% CO_2 as a product of steam reforming of methane or natural gas [33].

In order to compare the BCZY in the frame of proton conductor oxides, Table 3 shows some relevant information such as electrical conductivities, chemical stability, porosity, and sintering temperature of protonic conductors based on Ba-Ce-Zr composition. Despite the low grain boundary conductivity, BCZY shows high bulk protonic conductivity and good CO_2 tolerance compared with other proton conductors. These characteristics make this compound suitable to be used as (i) thin film as electrode supported SOFC to minimize grain boundary contribution [34] or as (ii) a buffer layer over another electrolyte with less CO_2 tolerance under low quality hydrogen [35].

4. Conclusion

The study of high temperature properties of $BaCe_{0.4}Zr_{0.4}Y_{0.2}O_{3-\delta}$ (BCZY) revealed a complex behavior below 500 °C with non-linear expansion, hysteresis loops and changes of electrical properties depending of the oxidizing/reducing character of atmosphere and the isotopic nature of the proton ions. HT-XRD, linear thermal expansion and TG data indicate the slope change and hysteresis for BCZY under oxidizing and reducing atmosphere, between 300 and 500° C, are associated with the incorporation/loss of interstitial protons. Significant change of grain boundary conductivity was observed for BCZY between experiments performed under oxidizing and reducing atmospheres. Furthermore, BCZY showed high bulk protonic conductivity and good CO_2 tolerance, so this compound could be used as electrolyte for PC-SOFC. The conductivity change under H_2O and D_2O oxidizing atmospheres reveals the transport nature of this material and its potential application as

isotopic separation membranes.

Acknowledgements

This work was supported by Departamento de Caracterización de Materiales, CAB - CNEA (Centro Atómico Bariloche - Comisión Nacional de Energía Atómica), CONICET (Consejo Nacional de Investigaciones Científicas y Técnicas), UNCu (Universidad Nacional de Cuyo), UNS (Universidad Nacional de Sur) and ANPCyT (Agencia Nacional de Promoción de Ciencia y Tecnología).

References

[1] E. Fabbri, D. Pergolesi, E. Traversa, Chem. Soc. Rev. 39 (2010) 4355.
[2] K.D. Kreuer, Annu. Rev. Mater. Res. 33 (2003) 333.
[3] R. Mukundan, E.L. Brosha, S.A. Birdsell, A.L. Costello, F.H. Garzon, R.S. Willms, J. Electrochem. Soc. 146 (1999) 2184.
[4] D. Medvedev, A. Murashkina, E. Pikalova, A. Demin, A. Podias, P. Tsiakaras, Prog. Mater. Sci. 60 (2014) 72.
[5] N. Nasani, P.A.N. Dias, J.A. Saraiva, D.P. Fagg, Int. J. Hydrogen Energy 38 (2013) 8461.
[6] P. Sawant, S. Varma, B.N. Wani, S.R. Bharadwaj, Int. J. Hydrogen Energy 37 (2012) 3848.
[7] L. Zhao, W. Tan, Q. Zhong, Ionics 19 (2013) 1745.
[8] Y. Guo, Y. Lin, R. Ran, Z. Shao, J. Power Sources 193 (2009) 400.
[9] S. Barison, M. Battagliarin, T. Cavallin, L. Doubova, M. Fabrizio, C. Mortalò, S. Boldrini, L. Malavasi, R. Gerbasi, J. Mater. Chem. 18 (2008) 5120.
[10] N. Nasani, D. Ramasamy, S. Mikhalev, A.V. Kovalevsky, D.P. Fagg, J. Power Sources 278 (2015) 582.
[11] J. Rodríguez-Carvajal, Phys. B 192 (1993) 55.
[12] J. Lagaeva, D. Medvedev, A. Demin, P. Tsiakaras, J. Power Sources 278 (2015) 436.
[13] J.F. Basbus, M. Moreno, A. Caneiro, L.V. Mogni, J. Electrochem. Soc. 161 (2014) F969.
[14] S. Megel, K. Eichler, N. Trofimenko, S. Hoehn, Solid State Ionics 177 (2006) 2099.
[15] http://compdent.uthscsa.edu/dig/itdesc.html.
[16] A. Caneiro, P. Bavdaz, J. Fouletier, J.P. Abriata, Rev. Sci. Instrum. 53 (1982) 1072.
[17] A. Caneiro, M. Chandrasekaran, Scr. Metall. 22 (1988) 1797.
[18] Zview versión 2.9b. Copyright 1990-2005, Scribner Associates, Inc. D. Johnson.
[19] C.-S. Tu, R.R. Chien, V.H. Schmidt, S.-C. Lee, C.-C. Huang, C.-L. Tsai, J. Appl. Phys. 105 (2009) 103504.
[20] M. Amsif, D. Marrero-López, J.C. Ruiz-Morales, S.N. Savvin, P. Núñez, J. Power Sources 196 (2011) 9154.
[21] A. Kruth, J.T.S. Irvine, Solid State Ionics 162–163 (2003) 83.
[22] Yu G. Lyagaeva, D.A. Medvedev, A.K. Demin, P. Tsiakaras, O.G. Reznitskikh, Phys. Solid State 57 (2015) 285.
[23] E. Gorbova, V. Maragou, D. Medvedev, A. Demin, P. Tsiakaras, J. Power Sources 181 (2008) 207.
[24] S. Yamaguchi, N. Yamada, Solid State Ionics 162 (2003) 23.
[25] X. Zhou, L. Liu, J. Zhen, S. Zhu, B. Li, K. Sun, P. Wang, J. Power Sources 196 (2011) 5000.
[26] D.A. Medvedev, J.G. Lyagaeva, E.V. Gorbova, A.K. Demin, P. Tsiakaras, Prog. Mater. Sci. 75 (2016) 38.
[27] A. Atkinson, S. Barnett, R.J. Gorte, J.T.S. Irvine, A.J. McEvoy, M. Mogensen, S.C. Singhal, J. Vohs, Nat. Mater. 3 (2004) 17.
[28] R. Glockner, M.S. Islam, T. Norby, Solid State Ionics 122 (1999) 145.
[29] N. Bonanos, Solid State Ionics 145 (2001) 265.
[30] K. Gdula-Kasica, A. Mielewczyk-Gryn, S. Molin, P. Jasinski, A. Krupa, B. Kusz, M. Gazda, Solid State Ionics 225 (2012) 245.
[31] D.A.G. Bruggeman, Ann. Phys. 5 (1935) 636.
[32] S. Ricote, N. Bonanos, G. Caboche, Solid State Ionics 180 (2009) 990.
[33] Z. Wang, J. Yang, Z. Li, Y. Xiang, Front. Energy Power Eng. China 3 (2009) 369.
[34] I. Chang, P. Heo, S.W. Cha, Thin Solid Films 534 (2013) 286.
[35] Y. Guo, R. Ran, Z. Shao, Int. J. Hydrogen Energy 35 (2010) 10513.
[36] W. Zając, E. Hanc, A. Gorzkowska-Sobas, K. Świerczek, J. Molenda, Solid State Ionics 225 (2012) 297.
[37] K.H. Ryu, S.M. Haile, Solid State Ionics 125 (1999) 355.
[38] A.K. Azad, J.T.S. Irvine, Chem. Mater. 21 (2009) 215.
[39] C. Zuo, S. Zha, M. Liu, M. Hatano, M. Uchiyama, Adv. Mater 18 (2006) 3318.